



Long-term global earth surface ultraviolet radiation exposure derived from ISCCP and TOMS satellite measurements

Pubu Ciren, Zhanqing Li*

Department of Meteorology, Earth and Space Science Interdisciplinary Center, University of Maryland, College Park, MD 20742, USA

Abstract

A long-term (1983–2000) global dataset of Earth's surface daily-integrated UV exposure was developed from a combination of ISCCP-D1 3 h reflectance measurements (in order to resolve the diurnal variation of cloud conditions) and TOMS total ozone amount. The inversion algorithm developed in our previous study was employed with modifications addressing the conversion of visible reflectance to UV albedo and narrowband UV albedo to broadband albedo over the range of 280–400 nm. Validation of the product was carried out using ground-based measurements at six stations. In general, good agreements between the estimated and measured daily UV exposure are found at most stations; the relative mean and root mean square (RMS) difference varies from 3 to 14% and from 20 to 45%, respectively. Among the stations, San Diego has a fairly low mean difference (9%) and the lowest RMS difference (33%), owing to the prevailing clear sky or uniform cloud cover condition. The RMS difference increases with cloud amount, which is largely caused by mismatch between satellite and ground-based measurements. The effect of diurnal variation in atmospheric opacity associated primarily with cloud on the estimation of daily erythemal UV doses is investigated with both ground-based measurements and ISCCP-D1 data. It is found that daily erythemal UV doses estimated from only a noontime satellite “snapshot” may incur errors larger than 20%, which may be reduced for long-term averaging.

© 2003 Elsevier B.V. All rights reserved.

Keywords: Albedo; Cloud cover; Total column ozone; Remote sensing; UV radiation; UVB

1. Introduction

Stratospheric ozone plays a crucial role in shielding the biosphere from the harmful ultraviolet radiation reaching the Earth's surface. As a major environmental issue, ozone depletion in the stratosphere (Stolarski et al., 1992) has invoked great concerns in both scientific communities and general public alike (Scotto et al., 1988; Bojkov, 1995). Consequently, numerous studies have been devoted to investigat-

ing the impact of such depletion on the potential increase of surface ultraviolet (UV) radiation exposure levels (Herman and Larko, 1994; Kerr and McElroy, 1993). The elevated UV exposure not only affects human health directly, but also has adverse effects on agriculture and forestry through reduction in yield and quality, alteration in species competition, decrease in photosynthetic activity, susceptibility to disease, and changes in plant structure and pigmentation (Tevini and Teramura, 1989; Bornman, 1989; Teramura and Sullivan, 1991). To fully assess these potential impacts requires a good knowledge of high-resolution global long-term UV radiation reaching the Earth's surface. Such a requirement cannot be met by ground-based observations alone since

* Corresponding author. Tel.: +1-301-405-6699; fax: +1-301-405-8468.

E-mail addresses: cpubu@essic.umd.edu (P. Ciren), zli@atmos.umd.edu (Z. Li).

they represent a very small portion of the Earth's surface.

Satellite estimation complements ground-based observations in that it provides global uniform coverage at high to moderate resolutions with consistent quality. However, satellite instruments cannot directly measure the amount of UV reaching the ground, but measures that reflected by the planet. Therefore, inversion algorithms or radiative transfer models are needed to infer the former from the latter by taking into account UV influential factors such as ozone amount, cloud and aerosol parameters, and surface reflectivity (Eck et al., 1987; Fredrick and Lubin, 1988; Eck et al., 1995; Herman and Celarier, 1997; Lubin et al., 1998; Krotkov et al., 1998; Herman et al., 1999; Li et al., 2000; Pubu and Li, 2001a).

While UV-caused damage to some components of the biosphere is proportional to the instant high UV exposure, a large amount of UV time-accumulated exposure is fatal to the survival of some life forms (Tevini, 1993). Hence a “snapshot” of UV intensity derived from a single satellite measurement, often offered by sensors aboard a sun-synchronous satellite, is insufficient to understand the ecological impact of the increased surface UV radiation. Daily-integrated UV radiation is needed to account for the diurnal variation of the UV dose rate caused primarily by changes in cloud conditions (Madronich, 1997). Various satellite sensors in the visible and infrared (IR) spectra have monitored cloud variability. The International Satellite Cloud Climatology Project (ISCCP) has compiled satellite measurements for nearly 20 years from a suite of operational satellites in polar-orbiting and geostationary platforms (Rossow and Schiffer, 1999). It contains global 3 h, daily, and monthly-averaged cloud parameters, including radiance data.

By integrating observations of cloud diurnal variation from sensors at wavelengths other than those at UV wavelengths with the total column ozone data measured by the total ozone measurement spectrometer (TOMS), the diurnal variation of the UV dose rate can be resolved. Lubin et al. (1998) combined TOMS monthly mean total ozone data with monthly hourly shortwave reflectance data from the earth radiation budget experiment (ERBE) to generate a global UV radiation climatology over a 4-year period (1985–1989). Another attempt at using multiple satellite data to derive surface UV dose rate was reported in Mayer and

Madronich (1998), where the 3 h cloud optical depth product from the ISCCP-D1 dataset and daily total ozone amount from Nimbus-7 over the period from 1989 to 1993 were employed. In both studies, radiative transfer models were used to calculate surface UV radiation based on the retrieved cloud optical depth and total ozone amount, together with other ancillary data.

In this study, a similar undertaking was pursued with a different approach (Li et al., 2000) that is particularly tailored to processing large volumes of satellite data with limited input parameters. This approach does not invoke any time-consuming radiative transfer calculations, and it thus avoids uncertainties associated with many input parameters that are needed for full radiative transfer modeling. The two most basic input parameters, namely, UV albedo at the top of the atmosphere (TOA) and column ozone amount can be estimated from ISCCP and TOMS. Aerosol optical depth and single scattering albedo are also input variables of the algorithm, but not critical especially for none or weak absorbing aerosols. In fact, the algorithm is not affected by conservative scattering aerosols at all, because their effect is inexplicitly accounted for by the TOA albedo, just like the effect of clouds. TOA UV albedo was estimated from the 3 h visible reflectance data of ISCCP-D1. No diurnal variation in ozone amount is assumed, because this value is derived from the once-per-day TOMS observation. The two data sets are introduced in the following section, together with ground-based UV observations that are employed for validation. Presented in Section 3 are the UV inversion algorithm of Li et al. (2000) and the newly developed visible (Vis)-UV reflectance conversion relationships. The adequacy of using 3 h sampling intervals in calculation of daily-integrated UV dose is evaluated, with respect to those computed from hourly ground-based measurements at several stations around the world. Daily-integrated erythemal UV doses and UV fluxes are estimated and compared with ground-based measurements. Differences are discussed.

2. Data and methods

2.1. Satellite data

As mentioned earlier, two satellite data sets are employed in this study, TOMS and ISCCP-D1. The

former provides total ozone amounts determined by the ratio of TOMS radiances measured at a pair of wavelengths of strong and weak (or no) ozone absorption bands in comparison with a pre-calculated lookup table generated by a radiative transfer model (McPeters et al., 1996). UV reflected radiances measured by TOMS were calibrated on board to assure the quality of its ozone retrievals. The TOMS ozone data have a daily global coverage over $1^\circ \times 1.25^\circ$ grids (latitude by longitude). TOMS has been operated nearly continuously since 1978 onboard NIMBUS-7 (1978–1993), METEOR-3 (1991–1994), ADEOS (1996–1997), and Earth Probe (1996–2003).

In generating the ISCCP dataset, TOA visible and IR radiance data were compiled from nearly all operational meteorological satellite sensors including the polar orbiting NOAA/AVHRR and geostationary GOES, GMS, and METEOSAT satellites. Cloud parameters, such as cloud fraction and optical depth were retrieved from satellite-measured radiance measurements. This study uses the calibrated visible reflectance data, rather than the retrieved cloud parameters. The ISCCP/D1 data has several improvements over an earlier version of the C-series data (Rossow and Schiffer, 1999; Trishchenko et al., 2001). Of most relevance to this investigation is a more accurate and consistent calibration (Brest et al., 1997). The total relative uncertainties in the radiance calibrations are estimated to be $\leq 5\%$ in the visible and $\leq 2\%$ in the infrared, while the absolute uncertainties are $< 10\%$ and $< 3\%$, respectively (Brest et al., 1997). The D1 dataset has a time interval of 3 h and is mapped on equal-area grids with a resolution of 280 km (Rossow et al., 1996). As of this writing, the released ISCCP-D1 data cover the period from 1983 to 2000. We will continue to generate the UV product, as new data from ISCCP and TOMS are made available to us.

2.2. Ground-based observations

The World Ozone and Ultraviolet Radiation Data Center (WOUDC) have compiled ozone and UV spectral measurements acquired by different institutes and agencies around the world. Unfortunately, only a small portion of this data can be matched in time and space with our satellite estimates, due to the limited overlap in both time and space between ISCCP-D1 measurements and the ground-based measurements used

in this study. Ground measurements employed in this study are mostly from Canada, US, and Japan Brewer spectrometers. Absolute calibration of these instruments was achieved through the use of a reference instrument that has a 1000 W lamp traceable to the NIST standard. Calibrations for the operational instruments were done annually for the Canadian stations and about every 3 years for the Japanese stations. Stability was checked daily with internal and external lamps. For the Canadian stations, wavelength registration was checked several times a day with reference to a mercury discharge lamp. The calibration uncertainty was 0.05 for wavelength and about 6–7% for intensity. Other quality control measures were also implemented. For example, a spectrum sample is flagged as unusual if the irradiance at 324 nm is lower than 13% of its “clear-sky value” or higher than 1.5 times this “clear-sky value”. The “clear-sky value” is defined as the 95th percentile of all measurements at the same solar elevation except those made with the presence of snow on the ground (Wardle et al., 1996). The flagged data were excluded from the final comparison in order to avoid using ground-based measurements acquired under rainy conditions or if the instrument was covered with snow.

3. Retrieval approach

3.1. Inversion algorithm

The inversion algorithm developed by Li et al. (2000) is adopted in this study to take advantage of its high efficiency and accuracy as demonstrated by Wang et al. (2000). However, a modification is made to take into account the effect of the varying Rayleigh scattering strength on the narrowband to broadband relationship, i.e. converting TOA albedo at 360 nm (R_{360}) to TOA mean albedo in the wavelength range from 280 to 400 nm without ozone absorption (R_{UV}). The algorithm is valid for retrieving surface UV quantities integrated over any interval with some coefficients to be adjusted accordingly. The algorithm is given by

$$UVB_{SFC}^{\downarrow} = \frac{UVB_{TOA}^{\downarrow} T_{O_3} ((1 - R_{UV}) - A_2) C}{1 - R_s} \quad (1)$$

$$C = \frac{(1 - R_s)}{(1 - R_s) + A_2^* R_s} \quad (2)$$

$$A_2 = 1 - \exp(-a_2\tau_e) \quad (3)$$

$$A_2^* = 1 - \exp(-b_2\tau_a) \quad (4)$$

$$\tau_a = (1 - \omega_0)\tau_e \quad (5)$$

$$T_{O_3} = \sum_{i=1}^n W_i \exp\left(-\frac{k_i O_3}{\mu_0}\right) \quad (6)$$

where UVB_{SFC}^{\downarrow} and UVB_{TOA}^{\downarrow} denote downwelling UV flux reaching the Earth's surface and UV flux incident on a horizontal surface at the TOA, respectively. T_{O_3} is the band-mean ozone transmittance. W_i and k_i represent the weight and ozone absorption coefficient in band i , respectively. O_3 and μ_0 are the total ozone amount (DU) and the cosine of the solar zenith angle (SZA). Absorption of downwelling and upwelling UV radiation due to aerosol are represented by A_2 and A_2^* , respectively. τ_e and τ_a represent total aerosol optical thickness and absorbing aerosol optical thickness. Aerosol absorption due to multiple scattering between the surface and the lower part of the atmosphere is accounted for by C . R_S and ω_0 denote, respectively, surface albedo and aerosol single-scattering albedo in the UVB wavelengths.

R_{UV} is the band-mean TOA albedo averaged across the UV wavelength (280–400 nm) under that condition of ozone-absorption free. The term $(1 - R_{UV})$ accounts for attenuation associated with scattering processes caused by atmospheric molecules, clouds, aerosol particles and the Earth's surface. This quantity has not been measured by any satellite sensor, but can be estimated from either TOMS 360 nm channel measurements or from a visible channel available from many space-borne sensors such as channel 1 of AVHRR. Li et al. (2000) found that the 360 nm narrowband albedo is highly correlated with the UV broadband TOA albedo. They proposed a linear conversion relationship to convert $R_{360} - R_{UV}$. A further investigation by Pubu and Li (2003) found that the use of the following non-linear relationship achieves more accurate results

$$R_{UV} = a + bR_{360}^c \quad (7)$$

where a , b , and c are coefficients that are functions of both the Rayleigh scattering optical depth and the solar zenith angle. Coefficients for erythemal UV dose rate are given in Table 1.

Table 1

The parameterization and coefficients used in Eq. (7).

EUV

$$a = aa_1 + bb_1 * \exp(-csza)/cc_1$$

$$aa_1 = -31.834 + 256.9881t_{ray} + 404.7636(t_{ray})$$

$$\times \log(t_{ray}) - 230.1488t_{ray}^3 + \frac{0.8048}{t_{ray}^{1.5}}$$

$$bb_1 = \frac{1}{1.7515 + 0.2641/\log(t_{ray})}$$

$$cc_1 = 0.2054 + 0.0829 \exp(-t_{ray}/-0.2378)$$

$$b = \frac{1}{aa_2 + bb_2/\sqrt{csza}}$$

$$aa_2 = 0.1483 + 0.9716 \exp(-t_{ray}/0.3542)$$

$$bb_2 = 2.5703 - 2.5870 \exp(-t_{ray})$$

$$c = aa_3 + bb_3 * (csza) (cc_3)$$

$$aa_3 = 2241.03 + 2529.23t_{ray} + 1382.8(t_{ray})^{2.5}$$

$$- 2275.36 \exp(t_{ray}) + 0.3846/(t_{ray})^2$$

$$bb_3 = 0.2578 + 19.0129(t_{ray})^{4.6366}$$

$$cc_3 = -1.9796 + 2.4246(t_{ray})^{0.8256}$$

*csza denotes the cosine of solar zenith angle. t_{ray} represents the optical depth of Rayleigh scattering at 350 nm.

Since the ISCCP dataset provides only TOA visible reflectance (R_{vis}), we need to apply both angular and spectral corrections to derive R_{360} . According to model simulations, R_{360} and R_{vis} are closely correlated and the correlation is dictated by two factors, namely, the spectral response function of the visible channel and the spectral function of the surface reflectivity. The former varies with satellite sensor used by ISCCP. All measurements used in ISCCP were initially normalized to conform to the spectral function of NOAA-7 (Brest and Rossow, 1992) and were later updated to conform to the spectral function of NOAA-9. Differences between the spectral response functions of the two radiometers are negligible. However, this is not the case for the surface effect due to the large variation in surface spectral reflectance on a global scale. Following a comprehensive investigation by radiative transfer modelling and analysis of coincident visible and UV measurements from various satellite sensors, Pubu and Li (2003) developed the following model to convert $R_{vis} - R_{360}$:

$$R_{360} = d + eR_{vis}^f \quad (8)$$

The coefficients were derived for different types of surface, such as water, dry sand, snow, and vegetation (deciduous, coniferous, and grass) that are given in Table 2. The effectiveness of this conversion is

Table 2

Dependence of the coefficients in Eq. (8) on the cosine of the solar zenith angle (csza) for four surface types: vegetation, water, snow and desert

Surface types	Coefficients
Vegetation	$d = 0.09805 + 0.6514e^{(-csza/0.5579)}$ $e = 0.6316 + 0.2072csza^{1.1311}$ $f = \sqrt{\frac{0.7741 + 0.5144}{csza^{1.5}}}$
Water	$d = 0.1248 + 0.6231e^{(-csza/0.5186)}$ $e = 0.6285 + 0.2csza^{1.0917}$ $f = \sqrt{\frac{0.8232 + 0.4717}{csza^{1.5}}}$
Snow	$d = 0.0$ $e = 1.0605 + 0.0217csza^{-1.1868}$ $f = 1.0$ $d = 0.7326 - 1.0409csza$ when $csza < 0.55$ $d = -0.1623 + 0.4696 \exp\left(\frac{-csza}{0.6443}\right)$ when $csza > 0.55$
Desert	$e = \frac{1}{1.2702 - 1.3325csza^3}$ when $csza < 0.55$ $e = \sqrt{1.752 - 1.1809 \exp(-csza)}$ when $csza > 0.55$ $f = -1.2937 + \frac{1.9189}{\sqrt{csza}}$ when $csza < 0.55$ $f = 1.0$ when $csza > 0.55$

*csza is the cosine of solar zenith angle.

not only demonstrated by comparing against simulations with a radiative transfer model (Pubu and Li, 2003), but also through comparisons of surface UV dose rates estimated from noontime TOMS 360 nm measurements and with those from noontime ISCCP visible measurements. The results of the latter comparisons over Toronto for the summer (May to September) of 1989–1992 are shown in Fig. 1. A close agreement is seen except for some very low dose rates associated with high solar zenith angles for which the plane-parallel radiative transfer models are generally not reliable. For stations that are located close to sea level, the modification to the narrowband to broadband conversion has relatively small effect on the validation results. However, up to 10–20% increase in the estimated surface UVB flux is possible for a region with surface pressure <700 mb.

Note that the UV inversion algorithm given by Eqs. (1)–(6) was not derived empirically, but was based on a simplified UV radiative transfer model. Despite its simplicity, its performance was satisfac-

tory when tested against extensive model simulation results obtained by a much more complex DISORT code under a wide range of atmospheric, cloud, and surface conditions (Li et al., 2000). Very good agreements were achieved in terms of both mean and root mean square (RMS) errors (Li et al., 2000). However, one variable was not taken into account in the original tests, namely, changes in the Rayleigh scattering optical depths due to varying surface elevation or surface pressure. Since this variable was not included as a model input, its influence was tested and the results are shown in Fig. 2. It is seen that the apparent dependence of UVB radiation on Rayleigh scattering optical depth is insignificant. This indicates that the effect of varying Rayleigh scattering is accounted for by the TOA albedo at 360 nm. Note that any change in the vertical ozone distribution associated with the rising elevation is not taken into account in this algorithm. However, the ensuing uncertainty was shown to be minor, especially for day-to-day variations in the surface UV dose (Krzysecin, 2000; Tsay and Stamnes, 1992), relative to errors incurred by variations in total ozone itself. In addition, the algorithm was also validated against instantaneous ground-based UV observational data (Wang et al., 2000).

4. Estimating daily-integrated UV doses

Using the aforementioned inversion algorithm, instantaneous UV fluxes and dose rates (UVB_{SFC}^{\downarrow}) are calculated every half-hour by changing the SZA while TOA albedos provided by ISCCP-D1 only vary in 3 h time intervals. The TOA reflectance measured from a particular viewing angle is first corrected for the bi-directional effect with the ERBE shortwave (SW) angular dependence model (ADM) (Suttles et al., 1988) in order to obtain a visible albedo defined over the upper hemisphere. The ADM for broadband SW albedo is, in general, very close to the visible ADM (Chang et al., 2000). Note that if TOMS UV reflectance data were used, one would apply the ADM developed specifically for UV radiation (Pubu and Li, 2001b). The visible albedo is then converted into a UV albedo at 360 nm using Eq. (7). Daily total ozone amounts from TOMS are used as input for computing instantaneous UV values with no consideration for diurnal variation. A monthly climatology

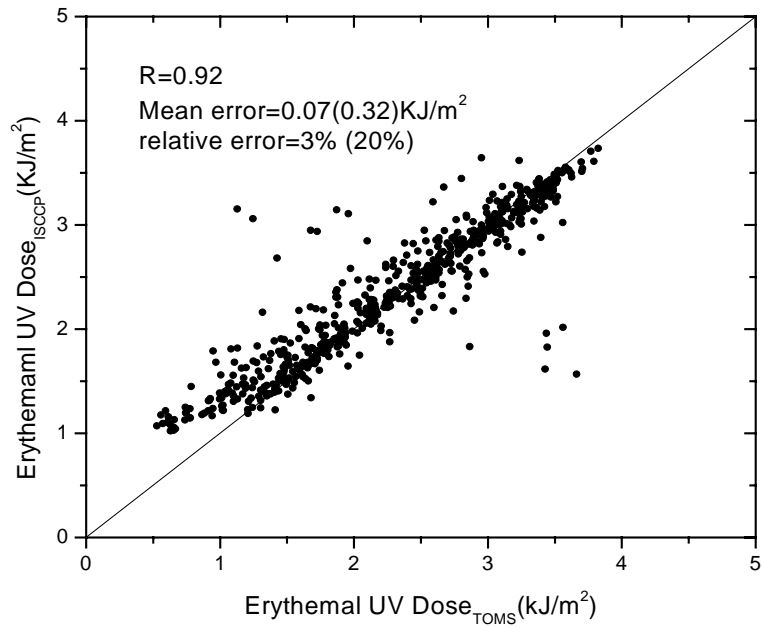


Fig. 1. Comparisons of daily-integrated erythemal UV doses estimated from TOMS-measured TOA 360 nm albedo with those estimated from the converted TOA 360 nm albedo from ISCCP close-to-noon visible reflectance, over Toronto during the summer (May–September) from 1989 to 1992. Mean and relative error and their standard deviations (shown in parenthesis) are also given.

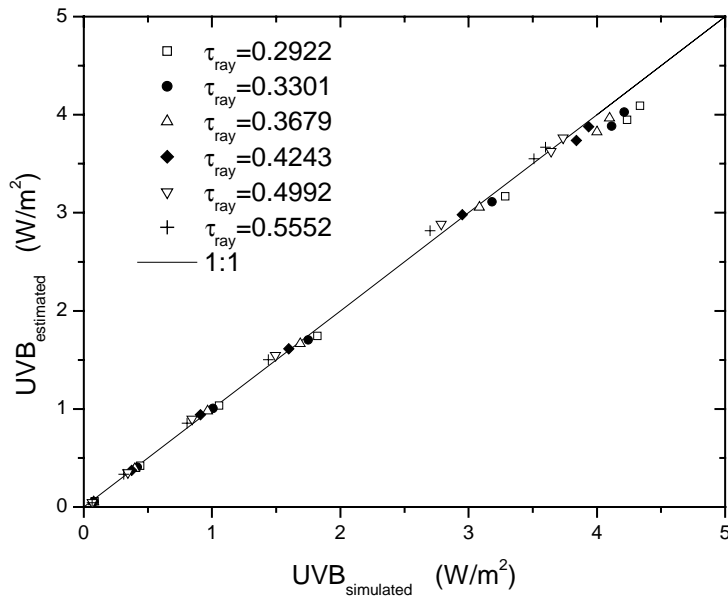


Fig. 2. Scatter plot of the estimated UVB flux against the model-simulated UVB flux for different Rayleigh scattering optical depths (τ_{ray}). Simulations were conducted for a mid-latitude summer atmospheric profile with a surface albedo of 0.05 and total ozone amount of 342 DU. The solar zenith angle (SZA) varies from 0 to 80.2°.

of surface albedo at 380 nm was generated by taking the minimum of the derived 380 nm scene reflectivities from 14.5 years' worth of TOMS measurements (Pubu and Li, 2001a). For snow/ice-covered grids, surface albedo is calculated as an average of TOMS-based values and 0.85 (representing snow/ice UV reflectivity), weighted by the snow/ice fraction from ISCCP-D1 data. From the instantaneous UV dose rate at each half-hour interval, daily UV dose (kJ/m^2) and UV flux were computed by integration.

4.1. Effect of diurnal variation due to clouds

Daily mean UV fluxes are driven by two major factors: the solar zenith angle and cloud diurnal variation. The former can be accurately accounted for, while the latter depends on both cloud variability and the number of measurements available. Daily mean UV doses derived from a single TOMS satellite measurement at local noon may be subject to large uncertainties, as is shown in Martin et al. (2000) using ground-based measurements. Errors over 20% often occur. However, the error decreases substantially (to <5%) for monthly mean values. Similar findings were reported by Lubin et al. (1998) using ERBE monthly–hourly measurements. Note that ERBE only has up to two satellites operated concurrently. The diurnal sampling problem is investigated here for the 3 h ISCCP data. To this end, we computed the following two transmittance-like terms:

$$R_1 = \sum_{i=1}^n [T_{O_3}(i) \times ((1 - a - b) \times (R_{360}(j))^c) \times \mu_0(i)] \quad (9)$$

$$R_2 = \sum_{i=1}^n [T_{O_3}(i) \times ((1 - a - b) \times (R_{360}(\text{noon}))^c) \times \mu_0(i)] \quad (10)$$

where $R_{360}(j)$ and $R_{360}(\text{noon})$ are the TOA 360 nm albedos at a particular 3 h time interval j and at, or close to, noon, respectively. They were calculated from visible albedos provided by the ISCCP-D1 measurements according to Eq. (8). $\mu_0(i)$ is the solar zenith angle at a half-hour time interval i and n is the total number of half-hour time intervals during the daytime. $T_{O_3}(i)$ is defined in Eq. (6). The total ozone amount is set at 350 DU. Note that the ratio of R_2 to R_1 is not very

sensitive to ozone amount. From Eqs. (1) and (6), it is evident that relative differences in the daily-integrated UV amount is proportional to the relative difference between R_1 and R_2 .

Fig. 3 shows the ratio of R_2 to R_1 as a function of TOA noontime visible albedo (hereinafter referred to as α_{vis}) for pixels covering eight ground stations, including the six stations used in the current study. There is a clear tendency for the ratio to generally decrease with increasing α_{vis} . Except for Barrow, San Diego, and Ushuaia, the correlation coefficients between the ratio and α_{vis} are fairly high, ranging from -0.71 to -0.85 . Yet, the ratio is generally larger (less) than unity for α_{vis} less (larger) than 0.15, implying that the daily erythemal UV dose would be overestimated using a single noontime ISCCP-D1 measurement made under clear or low cloud cover conditions. The opposite is true for overcast or thick cloud cover conditions. These results are similar to those obtained by Martin et al. (2000) with ground-based measurements. However, the magnitude of variation and scattering around the mean are considerably smaller for our results. This is probably because the large field-of-view of satellite measurements effectively smoothes out the large variation of local conditions, such as broken clouds. Moreover, the TOA visible albedos used in our study are more closely related to the optical properties of the troposphere than the ratio of the measured to the model-simulated clear-sky dose as used in the Martin et al. (2000) study. For the majority of the cases where there are clear skies and low cloud amounts, R_2 and R_1 agree with each other to within 20%. Statistical analyses for Fig. 3 indicate that the majority of the differences between R_2 and R_1 fall within a few percent for low and moderate TOA albedos, while differences larger than 20% may occur for high TOA albedo corresponding to heavy cloudy conditions at noon.

Table 3 presents similar results but for UV doses retrieved from satellite data at a 3 h interval versus single measurement made closest to noontime. The relative differences in the mean and RMS errors are given for satellite grids surrounding the six surface stations. It is seen that the mean relative differences are reduced, ranging from 0.3 to 2%. This is not surprising given the cancellation between positive and negative individual errors, as shown in Fig. 3. It is worth noting, however, that there is a consistent and

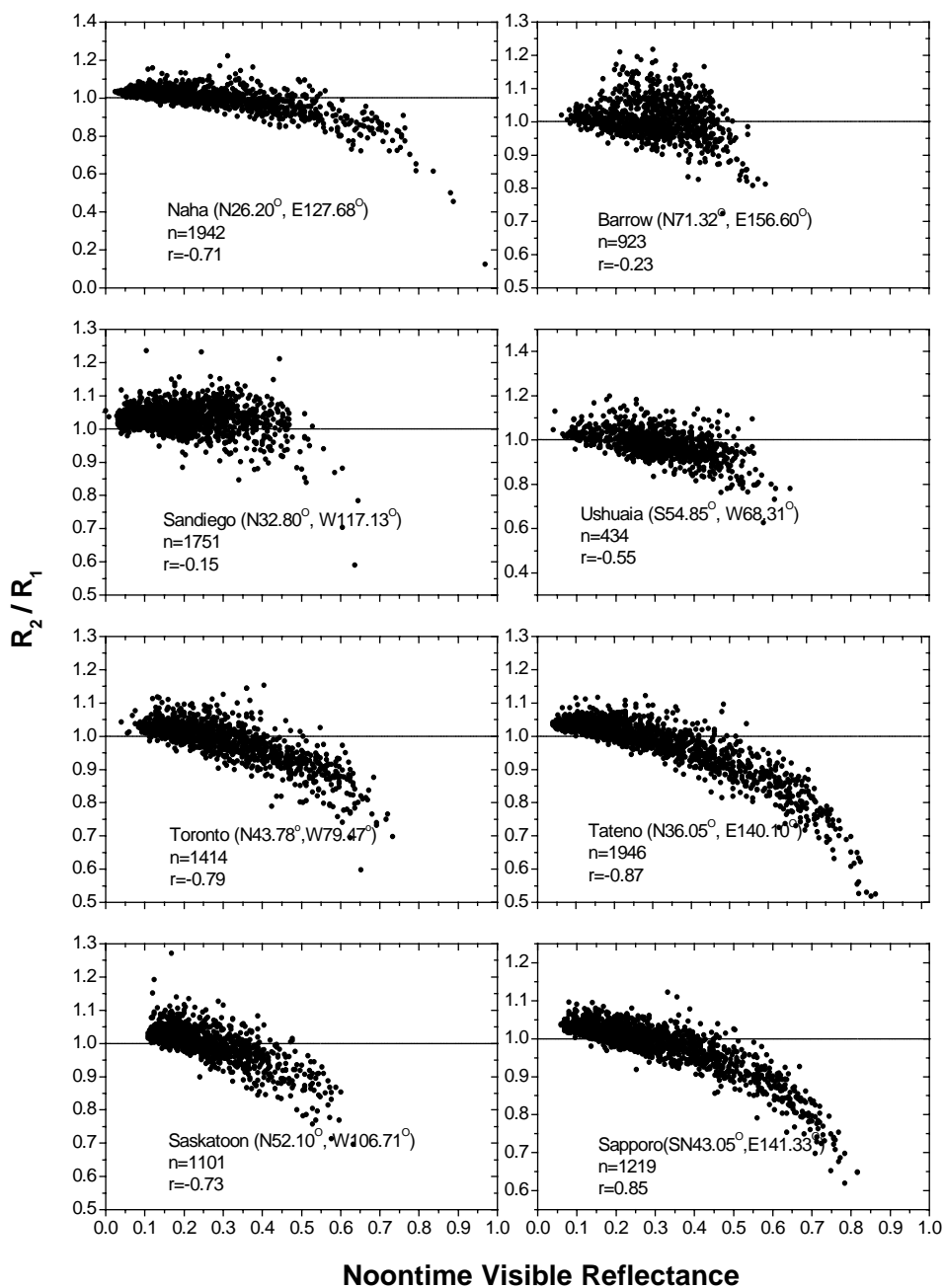


Fig. 3. Ratio of R_2 to R_1 as a function of TOA noontime visible reflectance. The number of samples (n) and the correlation coefficient (r) are also given.

Table 3

Comparison of the erythemal UV doses estimated from the ISCCP-D1 measurements at a single 3 h interval closest to noon-time (D_1) with that from measurements at all 3 h intervals (D_2)

Station	Difference ($D_1 - D_2$)/ D_1			
	r	mean (%)	rms (%)	n
Naha	0.99	-0.3	6	597
San Diego	0.99	1	4	143
Toronto	0.99	-2	6	793
Tateno	0.99	-2	9	818
Saskatoon	0.99	-0.6	5	535
Sapporo	0.99	-2	6	683

r and n denote the correlation coefficient and the number of samples, respectively.

significant reduction (5–10%) in RMS error, implying that individual daily UV dose rates estimated from ISCCP-D1 data are more accurate than those derived from a single measurement.

The interval of 3 h appears to be coarse when trying to resolve cloud diurnal variations. To further assess the degradation of accuracy due to this, comparisons are made between the daily erythemal UV doses calculated from ground-based measurements in two different sampling intervals, namely 3 h (in accord with the 3 h interval of the ISCCP-D1 data) and less than an hour, for the same eight stations as shown in Fig. 3. To ensure a sufficient number of samples during a day, only the days with at least 11 samples are selected, and the resulting daily erythemal UV doses are regarded as “ground truth”. Measurements acquired at a time closest to the median of a 3 h time interval was selected. Scatter plots of the daily erythemal UV doses calculated using these two sampling intervals are shown in Fig. 4. Overall, the two quantities agree well with each other with small mean and RMS differences. The slight underestimation (negative mean error) results from truncation errors incurred when integrating measurements of 3 h time duration using the trapezoid method. Reducing the time step of integration would alleviate this. In addition, note that these comparisons are based on ground-based measurements. Both the mean and RMS differences would be smaller in the estimates of daily erythemal UV dose over a satellite grid-box due to reduced cloud variability. It is thus concluded that 3 h sampling intervals suffice for estimating daily UV doses.

4.2. Global distribution of daily erythemal UV doses

With the method discussed earlier, global daily erythemal UV doses have been derived from July 1983 to April 1994. We are in the process of deriving the same data from 1994 to 2000. Continual processing for later years is planned, as ISCCP and TOMS data become available for later years. When the paper is published, we expect to have approximately 20 years of continuous surface instantaneous, daily and monthly mean UV doses. They will be made freely and readily available through the Internet service of the author’s institution (ESSIC) or upon request to the authors.

Plate 1 presents the global distribution of monthly means of daily erythemal UV doses for 4 months (January, April, July and October) in 1991. The geographic distribution of daily erythemal UV dose is a result of the combined effects due to variations in season, cloudiness, total ozone amount, aerosol content, and surface elevation. Among them, the seasonal variation, or more precisely, the change in SZA, is the dominant factor that drives the latitudinal pattern of daily erythemal UV doses. Limited by the lower resolution of ISCCP-D1 data ($2.5^\circ \times 2.5^\circ$ at the equator) and equal area mapping which gives an equivalent square cell of side 280 km, the details of the regional variation may not be seen in Plate 1. Large-scale features, however, are clearly visible. In general, it shows that the maximum daily erythemal UV dose is the highest over the subtropical high-pressure regions (where not only is the SZA small but the sky cloud-free) and decreases toward the poles. However, this pattern is disturbed by the regional variation of other factors, such as cloud cover. Relatively low values occur over cloudy regions such as the Inter-tropical Convergence Zone (ITCZ) in the tropics and during the monsoon season in India and China in July. Low values are also observed over the west coast of the United States in July due to the influence of persistent stratocumulus clouds. Besides cloud cover, surface elevation also significantly impinges upon the distribution of the daily erythemal UV dose by altering atmospheric scattering and total ozone amount (Xiuji and Cao, 1994; Han, 1996). According to the simulations of a radiative transfer model for a mid-latitude summer atmosphere, Pubu et al. (1999) found that elevating a surface from 0.0 to 3.5 km may enhance surface erythemal UV dose rate by 8–22% for a SZA ranging from 0 to 80° , with the

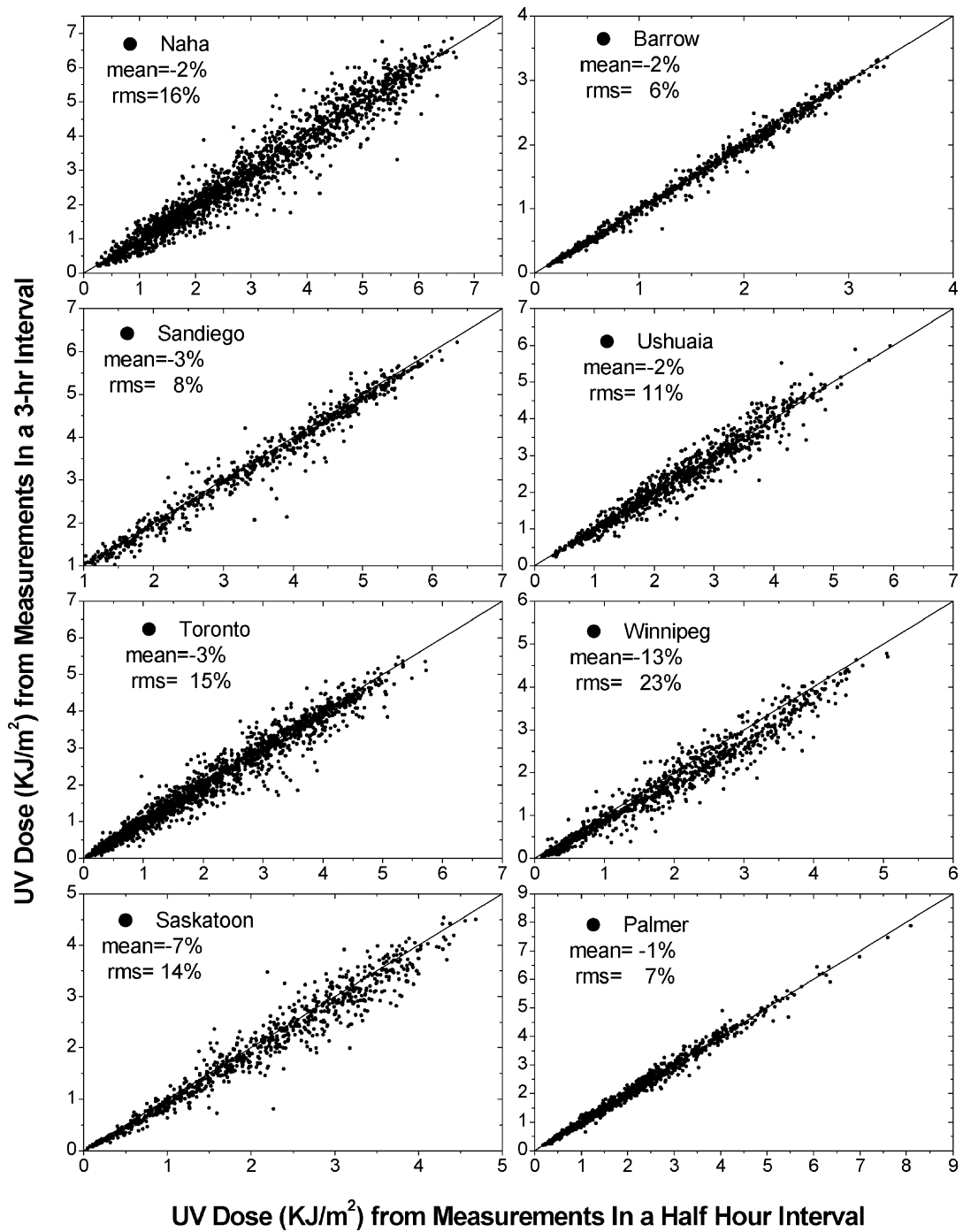


Fig. 4. Scatter plots of daily-integrated erythemal UV doses calculated from measurements by ground-based instruments during a time interval of <1 h against that from measurements by the same instrument during a time interval of 3 h. Relative mean and root mean square differences are marked.

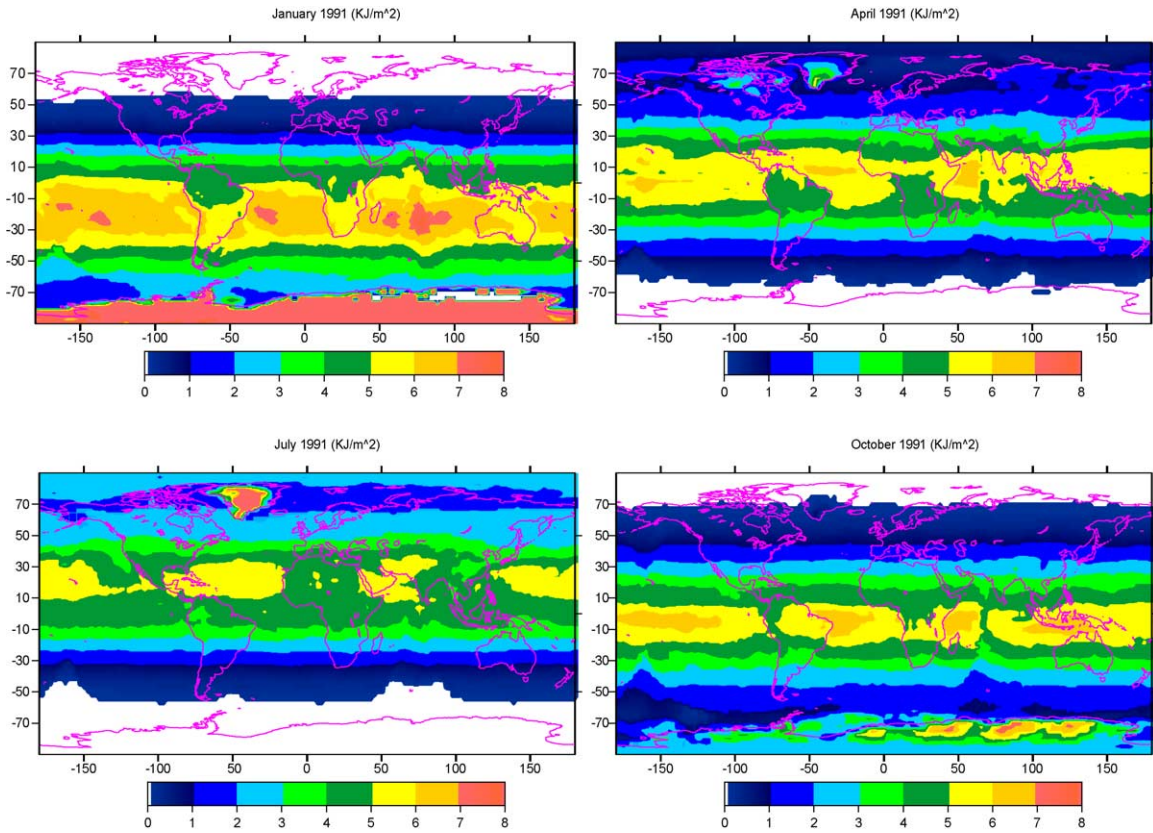


Plate 1. Global monthly mean daily erythemal UV doses derived from ISCCP-D1 and TOMS data for 1991 January (1), April (2), July (3) and October (4).

higher value corresponding to the higher SZA. It is clearly seen in Plate 1 that a high daily erythemal UV dose appears over the Andes Mountains in January and on the Tibetan Plateau in July.

As discussed above, a unique feature of the global daily erythemal UV doses derived from ISCCP-D1 data is the inclusion of the effect of diurnal variation in tropospheric opacity (mostly due to cloud cover). To examine this effect on a global scale, we calculated the relative difference between the monthly–daily erythemal UV doses in two different ways for January, April, July and October in 1991 (see Plate 2). One is based on all 3 h measurements (referred as EUV_{all}) and the other is from a single measurement closest to noon (referred as EUV_{noon}). Note that, to enhance the global distribution of the relative difference caused by sampling, only areas with more than three measurements (3 h intervals) per day are included. Hence, the spatial cover-

age is limited to within a latitude band between $\pm 65^\circ$, and most snow/ice cover areas are excluded. Over the oceans, it is noted that EUV_{all} are consistently lower by 3–8% than EUV_{noon} in the southeastern Pacific, the northeastern Pacific, and in the southeastern and tropical western Atlantic for nearly all seasons. In January and October, such a difference also appears over the southeastern Indian Ocean. Over land, EUV_{all} are consistently about 3–8% higher than EUV_{noon} over China, Japan, and Southeast Asia. In summer, over the western coast of the United States, a negative relative difference is spotted. In addition, larger EUV_{all} also appears in some regions over South America in January and October. The distribution patterns of the percentage differences shown in Plate 2 are similar to those reported by Lubin et al. (1998), attesting to the effect of differences in tropospheric opacity between morning and afternoon.

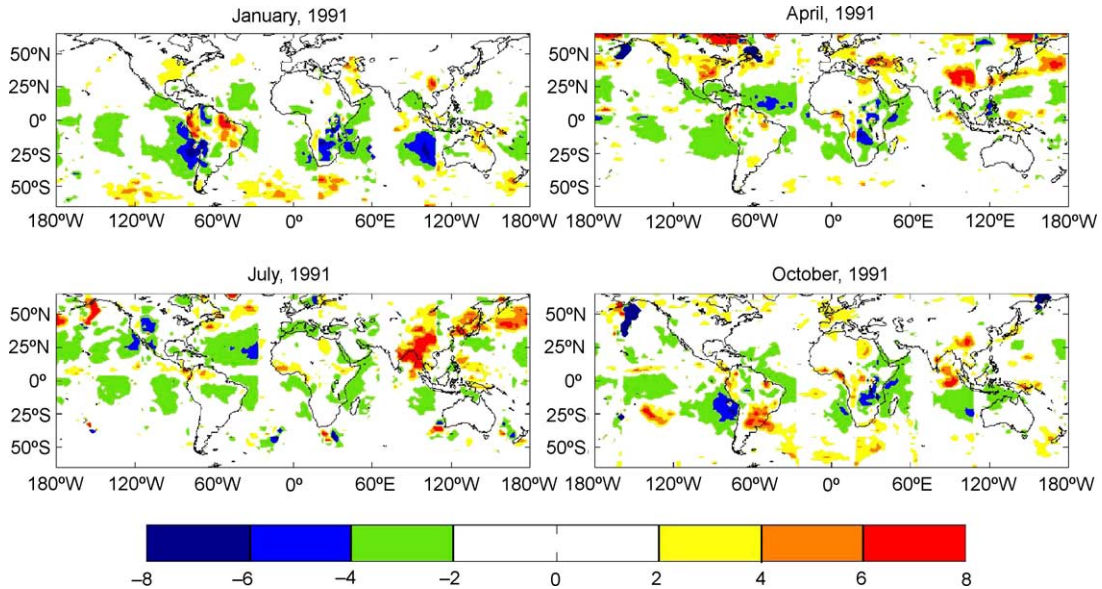


Plate 2. Percentage difference between daily erythemal UV doses estimated from all ISCCP-D1 3 h measurements and from midday measurements for the months of January, April, July and October of the year 1991. Polar regions are excluded due to less samples.

5. Validation against ground-based measurements

5.1. Daily-integrated erythemal UV dose and UVB flux

The quality of the estimated daily-integrated surface UV radiation from ISCCP-D1 satellite measurements is investigated by comparing them against those measured by ground-based instruments. Fig. 5 shows the comparisons of daily values for six stations with latitudes ranging from 26 to 52°N. These stations were selected because they had a sufficiently large number of observations matched in space and time with the ISCCP-D1 3 h measurements. Mean and RMS differences between satellite-estimated and ground-based data are also given in the figure, in both absolute (kJ/m^2) and relative magnitudes (%), and for all available data (shown at the upper left corner) and summer only (May to September) (at the lower right corner). It is seen that the estimates are closely correlated with the ground-based measurements with the correlation coefficient ranging from 0.75 to 0.96 for overall data (0.83 to 0.96 for the summer season). The systematic mean biases are also generally small, ranging from 0.1 to 0.4 kJ/m^2 and from 3 to 35%

in absolute and relative values, respectively, for the summer. Improvements are evident in terms of both the enhanced correlation and reduced scattering under summer conditions for most stations. However, the scattering of the data points is still rather significant with RMS values ranging from 29 to 78%. The scattering appears to be larger in low latitude stations such as Tateno and Naha. This is presumably because of more frequent cloud cover in low latitudes than in higher latitudes. Among the six stations shown in Fig. 5, San Diego has the highest correlation coefficient (0.96), a moderate mean difference (9%) and the lowest RMS of difference (33%), thanks to prevailing clear sky or uniform cloud cover conditions over this station.

The relatively large scattering is not surprising considering large differences in areas represented by ISCCP data (about $280 \text{ km} \times 280 \text{ km}$) and ground-based measurements (single point), and the strong spatial variation in the optical properties of the atmosphere and clouds. Therefore, instantaneous values measured by ground-based instruments at a single spot may deviate significantly from those estimated from satellite as a result of sampling errors. Due to the large difference in the spatial representation of an ISCCP-D1 grid box from that of a ground observation, the actual

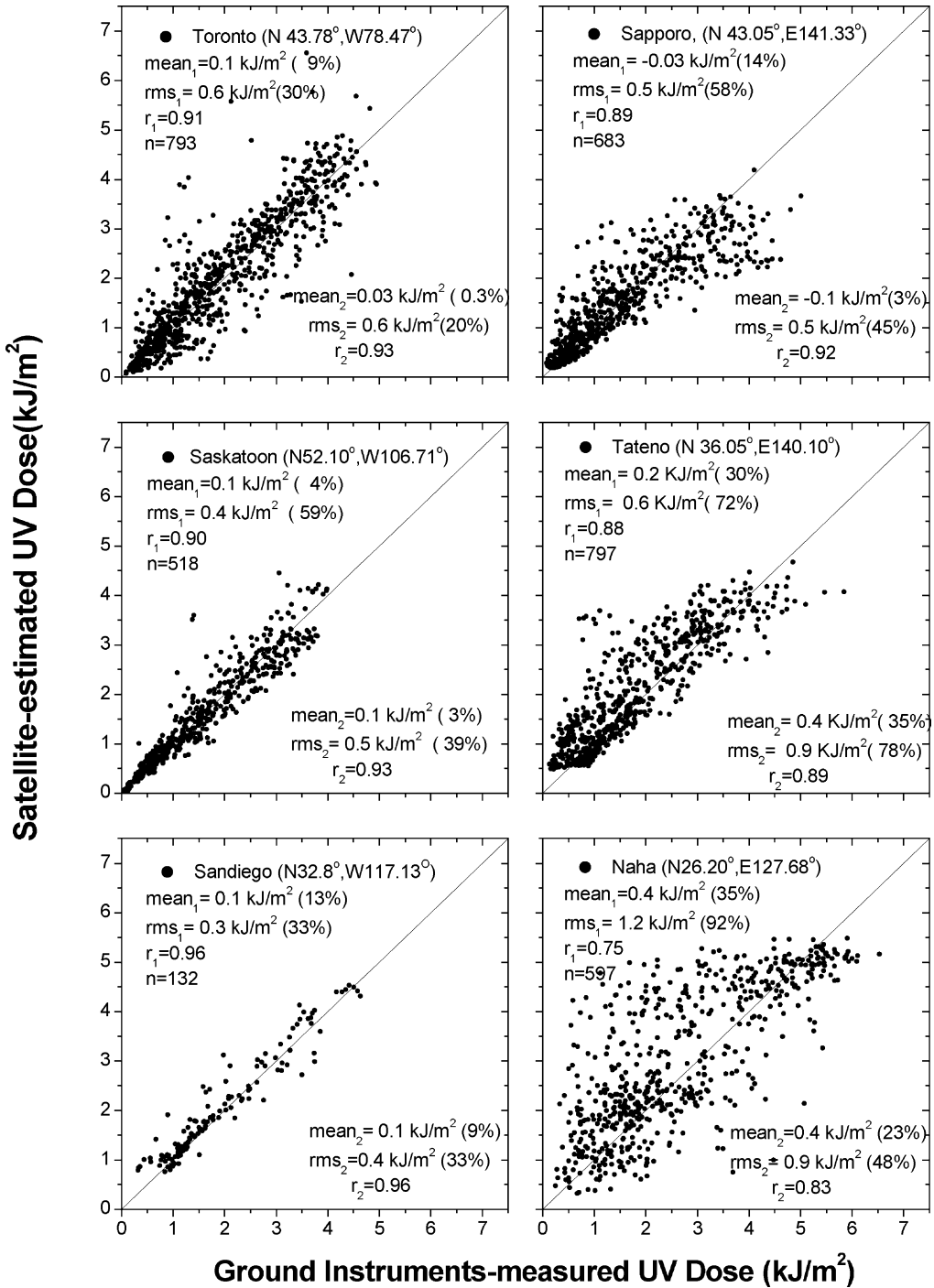


Fig. 5. Scatter plots of the daily-integrated erythemal UV doses estimated from ISCCP-D1 and TOMS measurements against those measured by ground-based instruments at six different stations. Statistics are shown for all available samples (upper left corner) and for snow-free samples (lower right corner).

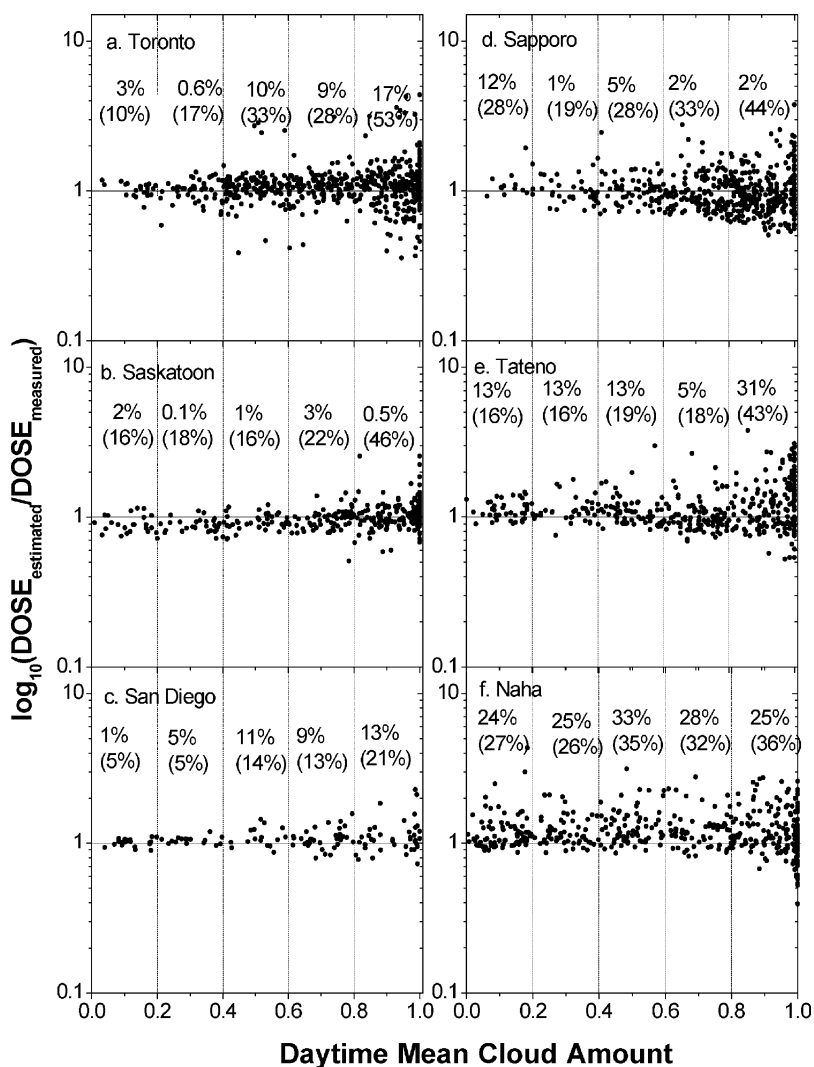


Fig. 6. Ratio of the satellite-based estimates of daily erythemal UV doses to ground-based measurements as a function of daily mean cloud amount in ISCCP-D1 pixels corresponding to ground stations. Mean and RMS differences (in parentheses) for the different bins of daily mean cloud amount are also shown.

magnitudes of the estimation errors would be reduced considerably if satellite retrievals and ground observations represented the same areas. This is demonstrated by the finding that the RMS errors in comparisons of the satellite-estimated and ground-measured surface insolation decrease substantially with increasing density of surface sites within a satellite grid cell (Li et al., 1995). In comparisons of instantaneous UVB irradiances from satellite estimations and ground-based observations, more scattering is found

under all-sky conditions than under clear-sky conditions (Wang et al., 2000). To check if this is the case for daily-integrated UV doses, Fig. 6 shows the variation of estimated-to-measured UV dose ratios against daytime mean cloud amount. The latter was calculated from daytime ISCCP-D1 3 h cloud statistics; the method for cloud detection was described by Rossow and Schifren (1999). Mean and RMS differences between the estimated and measured daily erythemal UV doses for different bins of daytime mean cloud

amount are also given. It is clearly seen that, except for Naha, the ratio is much more spread out at the high end of cloud amount than that at the lower end of cloud amount and that the RMS error differs by a factor of 2.

5.2. Monthly mean of daily erythemal UV doses

Averaging over a week or a month reduces the sampling error discussed above. This has been demonstrated for both TOMS-estimated UV irradiance (Herman et al., 1999) and TOMS-estimated daily erythemal UV dose (Kalliskota et al., 2000). The same is true for our ISCCP-TOMS based estimates of erythemal UV doses, as shown in Figs. 7 and 8. Fig. 7 presents the daily variations of erythemal UV dose in the grid-cell encompassing Toronto in 1991, in comparison with ground measurements. Individual dots (solid for ground observations and open for satellite estimations) correspond to daily mean values, while the curves are for 7-day running means. As the interval of temporal averaging increases from 1 to 7 days, the correlation coefficient increases from 0.95 to 0.98 and RMS relative differences decrease from

61 to 19%. Unlike other time periods, overestimation appears around February and March. This is probably because there is subgrid-scale snow cover in the ISCCP-D1 grid, leading to a surface albedo that is too high and not representative of the ground condition at the site. The correlation coefficients between estimated and observed UV doses ranges from 0.89 to 0.97 in summer (May to September) and from 0.83 to 0.85 in winter (all other months); this corresponds to relative RMS differences of 19–10% (summer) and 83–24% (winter), respectively. This finding is similar to that of Kalliskota et al. (2000). It is also noted that the overall mean bias reduces from 11 to 3% after 7-day running averaging. The reduction is attributed primarily to wintertime data, for which the mean bias is reduced from 18 to 6%. The running average has almost no effect (from 1.2 to 0.7%) during the summer. This is related to the surface condition, which is more variable in winter than in summer due to inhomogeneous snow cover.

After taking monthly averages, as shown in Fig. 8, there is an overall improvement in the agreement between the satellite-estimated and ground-based measurements, relative to Fig. 7. For example, for Naha,

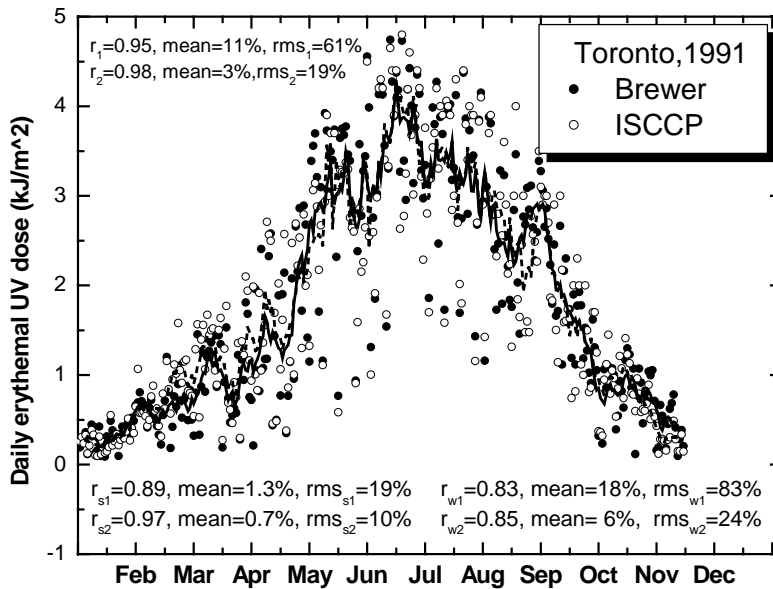


Fig. 7. Comparisons of the seasonal variation of daily erythemal UV doses (\circ) estimated from satellite and measured at ground (\bullet) in Toronto in 1991. The 7-day running averages are also shown for satellite estimates (thick solid line) and ground-based measurements (dashed line). The correlation coefficients and root mean square errors for the comparisons before and after the 7-day running averages are denoted by r_1 (or rms_1) and r_2 (or rms_2).

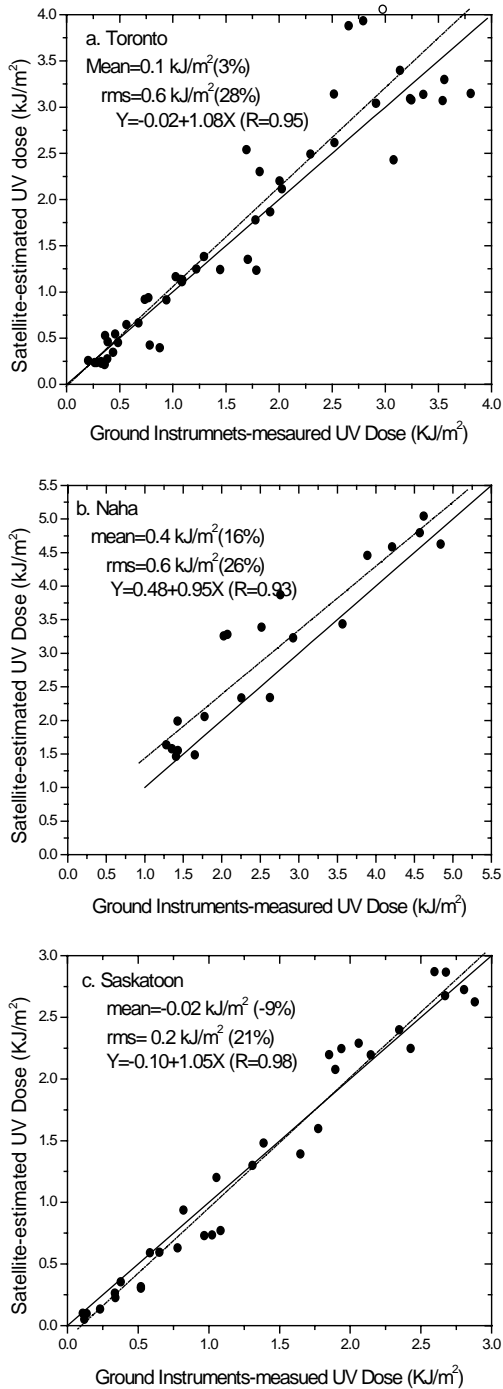


Fig. 8. Scatterplots of the monthly means of satellite-based estimates of erythemal UV doses against ground-based measurements.

the correlation coefficient increases from 0.75 to 0.97, while the mean and RMS of the relative differences are reduced from 35 to 16% and from 92 to 26%, respectively. Averaging does not alter the mean bias significantly.

6. Summary

Satellite-based remote sensing offers a practical means of monitoring and mapping UV radiation reaching the Earth's surface on a large scale. In this study, we applied a simple but efficient inversion algorithm to ISCCP-D1 and TOMS data in order to generate a long-term global climatology of surface UVB and dose rates. ISCCP data provides TOA reflectance measurements at a time interval of 3 hours, allowing to better account for the diurnal variation caused primarily by cloud.

Since the UV algorithm of Li et al. (2002) requires UV broadband albedo at the TOA, spectral and angular conversions are necessary to transform ISCCP-D1 reflectance data into UV albedo. To this end, we first used the ERBE ADM which is very close to visible ADM (Chang et al., 2000) to obtain TOA visible albedo. The visible albedo is then converted to TOA albedo at 360 nm and across the UV wavelengths (280–400 nm) using a new set of relationships derived by means of radiative transfer modelling for four typical surface types (vegetated land, water, desert and snow). Relative to a single relationship applied to all types of surfaces, errors in estimated erythemal UV dose rate incurred due to the spectral conversion diminish from $\pm 20\%$ to less than $\pm 5\%$.

Daily-integrated UV doses have been derived from a single TOMS measurement around noon. To investigate uncertainties resulting from the diurnal variation of cloud cover, we compared the daily erythemal UV dose calculated from single ISCCP-D1 measurements made around noon to that calculated from all ISCCP-D1 measurements. It was found that the errors are insignificant for long-term average quantities, such as monthly means of daily erythemal UV doses, but rather large ($>20\%$) for daily means.

Applying the algorithm to a combination of ISCCP and TOMS data, a long-term (~ 20 years) global UV climatology was developed that includes instantaneous, daily, and monthly mean values. The derived

daily erythemal UV doses are validated against ground-based measurements at six stations. In general, good agreements are found between the estimated and measured UV doses for most stations. The mean and RMS differences range from 3 to 14% and from 20 to 45%. There are better agreements under clear-sky conditions than under cloudy-sky conditions. RMS differences usually increase with increasing cloud amount within the ISCCP grid. The best agreement was achieved at San Diego where cloudless sky or a uniform cloud cover prevails. The corresponding mean and RMS differences are 9 and 33%, respectively. A considerable portion of the differences originates from the mismatch between satellite and ground-based measurements. This new comprehensive data set may be useful for a variety of studies including investigations on the biological and ecological effect of UV radiation reaching the Earth's surface.

Note that our data set differs from a similar product generated at NASA/GSFC (Herman et al., 1999) in many regards including use of different inversion algorithm and input data. A preliminary comparison of the two data sets reveals similar spatial and temporal variations, but systematic discrepancies in magnitude by about 15%. This is consistent with the differences between their estimates and ground observations. In Toronto, for example, the difference is about 20% and about 6% is caused by Brewer cosine response error (Herman et al., 1999; McKenzie et al., 2001). Since our ISCCP-based estimates of UV TOA albedo are very close to the TOMS direct measurements (c.f. Fig. 1), the systematic difference seems more likely associated with the different inversion algorithms used. A further investigation is thus warranted to compare and pinpoint the discrepancy between the two inversion algorithms, as well as the ensuing products.

Acknowledgements

This study was partially supported by the Department of Energy's Atmospheric Radiation Measurement (ARM) program under a grant DEFG0201-ER63166 and partially by the National Science Foundation of China (NSFC40028503). We are very grateful to the guest editor, Dr. Gordon Heisler, and three anonymous reviewers whose comments helped improve the quality of the paper.

References

- Bojkov, R.D., 1995. The changing ozone layer. Publication World Meteorological Organization, Geneva, ISBN 92-63-10828-5.
- Bornman, J.F., 1989. Target sites of UV-B radiation in photosynthesis of higher plants. *J. Photochem. Photobiol. B: Biol.* 4, 145–158.
- Brest, C.L., Rossow, W.B., 1992. Radiometric calibration and monitoring of NOAA AVHRR data for ISCCP. *Int. J. Remote Sens.* 13, 235–273.
- Brest, C.L., Rossow, W.B., Roiter, M.D., 1997. Update of radiance calibrations for ISCCP. *J. Atmos. Ocean Technol.* 14, 1091–1109.
- Chang, F.-L., Li, Z., Trishchenko, A., 2000. The dependence of TOA anisotropic reflection on cloud properties inferred from ScaRaB satellite data. *J. Appl. Meteorol.* 39, 2480–2493.
- Eck, T.F., Bhartia, P.K., Wang, P.H., Stowe, L.L., 1987. Reflectivity of Earth's surface and clouds in ultraviolet from satellite observations. *J. Geophys. Res.* 92, 4287–4296.
- Eck, T.F., Bhartia, P.K., Kerr, J.B., 1995. Satellite estimation of spectral UVB irradiance using TOMS derived ozone and reflectivity. *Geophys. Res. Lett.* 22, 611–614.
- Fredrick, J.E., Lubin, D., 1988. The budget of biologically effective ultraviolet radiation in the earth-atmosphere system. *J. Geophys. Res.* 93, 3825–3832.
- Han, Z., 1996. Seasonal variation and trends of TOMS ozone over Tibet. *Geophys. Res. Lett.* 23, 1029–1032.
- Herman, J.R., Larko, D., 1994. Low ozone amounts during 1992 and 1993 from Nimbus 7 and Meteor 3 total ozone mapping spectrometers. *J. Geophys. Res.* 99, 3483–3496.
- Herman, J.R., Celarier, E., 1997. Earth surface reflectivity climatology at 340–380 nm from TOMS data. *J. Geophys. Res.* 102, 28,003–28,012.
- Herman, J.R., Krotkov, N., Celarier, E., Larko, D., Labow, G., 1999. Distribution of UV radiation at the Earth's surface from TOMS-measured UV-backscattered radiances. *J. Geophys. Res.* 104, 12,059–12,076.
- Kalliskota, S., Kaurola, J., Taalas, P., Herman, J.R., Celarier, E.A., Krotkov, N.A., 2000. Comparison of daily UV doses estimated from Nimbus-7/TOMS measurements and ground-based spectroradiometric data. *J. Geophys. Res.* 105, 5059–5067.
- Kerr, J.B., McElroy, C.T., 1993. Evidence for large upward trends of ultraviolet-B radiation linked to ozone depletion. *Science* 262, 1032–1034.
- Krotkov, N.A., Bhartia, P.K., Herman, J.R., Fioletov, V., Kerr, J., 1998. Satellite estimation of spectral surface UV irradiance in the presence of tropospheric aerosols. Part 1. Cloud-free case. *J. Geophys. Res.* 103, 8779–8793.
- Krzyscin, J., 2000. Impact of the ozone profile on the surface UV radiation: analysis of the Umker and UV measurements at Belsk, Poland. *J. Geophys. Res.* 105, 5009–5015.
- Li, Z., Wang, P., Cihlar, J., 2000. A simple and efficient method for retrieving surface UV dose rates. *J. Geophys. Res.* 105, 5027–5036.
- Lubin, D., Jensen, E.H., Gies, H.P., 1998. Global surface ultraviolet radiation climatology from TOMS and ERBE data. *J. Geophys. Res.* 103, 26061–26091.

- Mckenzie, Seckmeyer, R.G., Bais, A., Kerr, J., Madronich, S., 2001. Satellite-retrievals of erythemal UV dose compared with ground-based measurements at Northern and Southern mid-latitudes, *J. Geophys. Res.* 106, 24051–24062.
- Martin, T.J., Gardiner, B.G., Seckmeyer, G., 2000. Uncertainties in satellite-derived estimates of surface UV dose. *J. Geophys. Res.* 105, 27005–27011.
- Madronich, S., 1997. Theoretical estimation of biologically effective UV radiation at the Earth's surface, solar ultraviolet radiation: modeling, measurements and effects. NATO ASI Series, Series 1: Global Environmental Change 52, 23–47. Springer.
- Mayer, B., Madronich, S., 1998. Calculation of ultraviolet radiation quantities using TOMS ozone and ISCCP cloud data. *EOS Trans.* 79, F170.
- McPeters, R.D., Krueger, A.J., Bhartia, P.K., Herman, J.R., et al., 1996. "Nimbus-7 total ozone mapping spectrometer (TOMS) Data Products User's Guide", vol. 301, NASA Reference Publication 1384. NASA Center for AeroSpace Information, 800 Elkridge Landing Road, Linthicum Heights, MD 21090, USA, p. 621-0390.
- Pubu, C., Gjessing, Y., Sigernes, F., 1999. Measurements of solar ultraviolet radiation on the Tibetan Plateau and comparisons with discrete ordinate method model simulation. *J. Atmos. Solar Terrestrial Phys.* 61, 425–446.
- Pubu, C., Li, Z., 2001a. Satellite Remote Sensing of Surface UV Fluxes and Albedo from TOMS and ISCCP Measurements, *IRS2000: Current Problems in Atmospheric Radiation*, A. Deepak Publishing, pp.129–132.
- Pubu, C., Li, Z., 2001b. Anisotropic reflection of UV radiation at the top of the atmosphere: characteristics and models obtained from Meteor-3/TOMS. *J. Geophys. Res.* 106, 4741–4755.
- Pubu, C., Z. Li, 2003. An Improved Method to Estimate Surface UV Radiation from Satellite Data: Narrowband to Broadband Conversion. (in press).
- Rosow, W., Schiffer, R., 1999. Advances in understanding clouds from ISCCP. *Bull. Am. Meteorol. Soc.* 80, 2261–2284.
- Rosow, W., Walker, A.W., Beuschel, D., Roiter, M., 1996. International Satellite Cloud Climatology Project (ISCCP) description of new cloud dataset, WMO/TD 736, World Climate Research Program (ICSU and WMO), 115 pp.
- Scotto, J., Cotton, G., Urbach, F., Berger, D., Fears, T., 1988. Biologically effective ultraviolet radiation: surface measurements in the United States, 1974 to 1985. *Science* 239, 762–764.
- Stolarski, P., Bojkov, R., Bishop, L., Zerefos, C., Staehelin, J., Zawodny, J., 1992. Measured trends in stratospheric ozone. *Science* 256, 342.
- Suttles, J.T., Green, R.N., Minnis, P., Smith, G.L., Staylor, W.F., Wielicki, B. A., Walker, I.J., Young, D.F., Taylor, V.R., Stowe, L.L., 1988. Angular radiation models for Earth-atmosphere system. Part I. Shortwave radiation, vol. 1184. NASA Reference Publication, 144 pp.
- Tevini, M., Teramura, A.H., 1989. UV-B effects on terrestrial plants. *Photochem. Photobiol.* 50, 479–487.
- Tevini, M. (Ed.), 1993. *UVB Radiation and Ozone Depletion: Effects on Humans, Animal, Plants, Microorganism, and Materials*. Lewis Publishers, Boca Raton.
- Teramura, A.H., Sullivan, J.H., 1991. Potential effects of increased solar UV-B on global plant productivity. In: E. Riklis (Ed.), *Photobiology*. Plenum Press, New York, pp. 625–634.
- Trishchenko, A.P., Li, Z., Chang, F.-L., 2001. Cloud optical depths and TOA fluxes: comparison between satellite and surface retrievals from multiple platforms. *Geophys. Res. Lett.* 28, 979–982.
- Tsay, S.C., Stamnes, K., 1992. UV radiation in the Arctic: the impact of potential ozone depletions. *J. Geophys. Res.* 97 (D8), 7829–7840.
- Wang, P., Li, Z., Wardle, D., 2000. Validation of UVB inversion algorithm using satellite and surface measurements. *J. Geophys. Res.* 105, 5037–5048.
- Wardle, D.I., Hare, E.W., Barton, D.V., McElroy, C.T., 1996. The World Ozone and Ultraviolet Radiation Data Centre—Content and Submission. In: *Proceedings of the XVIII Quadrennial Ozone Symposium*, L'Aquila, Italy, 12–21 September 1996.
- Xiuji, Z., Cao, L., 1994. Ozone valley over Tibetan Plateau. *Acta Meteorol. Sinica* 8 (4), 505–506.